Influence of polymer additives on turbulent energy cascading in forced homogeneous isotropic turbulence studied by direct numerical simulations*

Li Feng-Chen(李凤臣), Cai Wei-Hua(蔡伟华)†, Zhang Hong-Na(张红娜), and Wang Yue(王 悦)

School of Energy Science and Engineering, Harbin Institute of Technology, Harbin 150001, *China*

(Received 15 April 2012; revised manuscript received 8 May 2012)

Direct numerical simulations (DNS) were performed for the forced homogeneous isotropic turbulence (FHIT) with/without polymer additives in order to elaborate the characteristics of the turbulent energy cascading influenced by drag-reducing effects. The finite elastic non-linear extensibility-Peterlin model (FENE-P) was used as the conformation tensor equation for the viscoelastic polymer solution. Detailed analyses of DNS data were carried out in this paper for the turbulence scaling law and the topological dynamics of FHIT as well as the important turbulent parameters, including turbulent kinetic energy spectra, enstrophy and strain, velocity structure function, small-scale intermittency, *etc.* A natural and straightforward definition for the drag reduction rate was also proposed for the drag-reducing FHIT based on the decrease degree of the turbulent kinetic energy. It was found that the turbulent energy cascading in the FHIT was greatly modified by the drag-reducing polymer additives. The enstrophy and the strain fields in the FHIT of the polymer solution were remarkably weakened as compared with their Newtonian counterparts. The small-scale vortices and the small-scale intermittency were all inhibited by the viscoelastic effects in the FHIT of the polymer solution. However, the scaling law in a fashion of extended self-similarity for the FHIT of the polymer solution, within the presently simulated range of Weissenberg numbers, had no distinct differences compared with that of the Newtonian fluid case.

Keywords: forced homogenous isotropic turbulence, polymer additives, turbulent energy cascading, drag reduction

PACS: 47.27.Gs, 47.50.–d, 47.85.lb **DOI:** 10.1088/1674-1056/21/11/114701

1. Introduction

It has been known for a long time that the addition of minute amounts of flexible long-chain polymers or some kinds of surfactants to a Newtonian fluid flow can significantly modify its flow properties. This can lead to a dramatic frictional drag reduction (DR) in the wall turbulence at a high Reynolds number.[1−9] In a flow of aqueous solution of long-chain polymers, viscoelasticity is introduced by the stretching of polymer molecules by the velocity gradient. Alternatively, viscoelasticity is introduced in a flow of drag-reducing surfactants by the shear-induced microstructures formed by the rod-like micelles. We can qualitatively say that the underlying mechanism behind the DR is the interaction between the viscoelasticity and the turbulence structures.

Since the discovery of the DR phenomenon several decades ago, a large amount of studies on the characteristics of drag-reducing wall-turbulent flows of viscoelastic fluids and the mechanism of the DR have been carried out. Some consensuses have been obtained in the study of several effects. The viscoelasticity generated by the drag-reducing additives damps the fluctuation of the velocity component normal to the wall, enhances that of the streamwise velocity (normalized with the inner variables), greatly decreases the Reynolds shear stress, increases the space between the near-wall low-speed streaks, and so on.[4,7−16] Due to the inhomogeneous nature caused by the wall effect, however, the wall-bounded turbulent flow seems to be unsuitable to be used for analyzing the interaction between the pure turbulence and the micro-structures existing in the drag-reducing solutions. In contrast, it is much more straightforward to study the turbulence–microstructures interaction

*Project supported by the National Natural Science Foundation of China (Grant Nos. 51076036 and 51206033), the Foundation for Innovative Research Groups of the National Natural Science Foundation of China (Grant No. 51121004), the Fundamental Research Funds for the Central Universities, China (Grant No. HIT.BRET2.2010008), the Doctoral Fund of Ministry of Education of China (Grant No. 20112302110020), and the China Postdoctoral Science Foundation (Grant No. 2011M500652).

†Corresponding author. E-mail: caiwh@hit.edu.cn

© 2012 Chinese Physical Society and IOP Publishing Ltd

based on a homogeneous isotropic turbulence (HIT) without the wall effect.

Indeed, there have been some studies performed on the HIT with the drag-reducing effects, though the number of such studies is much smaller than those on the drag-reducing turbulent wall-bounded flows. It was found that there are some remarkable changes in the grid-generated turbulence in the dilute polymer solution as compared with its Newtonian fluid counterpart, such as a significant alteration of turbulent kinetic energy distribution among scales[17,18] and energy budget,[19] a smaller dissipation rate,[20] a suppression of small-scale structures, and a truncation of energy cascade.[20,21] The above experimental studies of the grid turbulence in the dilute polymer solution suggested that the DR also exists even in situations where the wall plays no apparent role.

Recently, the direct numerical simulation (DNS) of the HIT with polymer additives has become an important tool to study the additives–turbulence interaction and the physical mechanism of the DR. The two most frequently studied cases of isotropic turbulence are the freely decaying HIT (DHIT) and the forced (statistically stationary) HIT (FHIT). In the DHIT with polymer additives, some interesting results have been obtained, such as a remarkable alteration of the turbulent kinetic energy spectrum, the reduction of both viscous dissipation and intermittency in the dissipation range, and the inhibition of small-scale structures.[22,23] In a very recent DNS study on the DHIT with polymer additives,[24,25] we found that in the DHIT with polymer additives, (i) the decay of the turbulent kinetic energy is faster than that in the Newtonian fluid case; (ii) the classical Kolmogorov energy cascade is modified due to the release of the polymer elastic energy into the flow structures at some certain small scales in the polymer solution case; (iii) the enstrophy and the strain are both smaller than those in the Newtonian fluid case, and the polymer effects on these two variables behave negatively; (iv) the stretching or compressing strength of the flow field is weakened in all directions determined by the eigenvectors of the rate-of-strain tensor due to the polymer's effect; (v) analogous to the relationship between vorticity and rate-of-strain tensor, the vorticity tends to be aligned with the first and the intermediate eigenvectors of the polymer conformation tensor, especially with the intermediate eigenvector.

However, it is impossible to obtain statistically stationary quantities in the DHIT, such as turbulent kinetic energy, turbulent energy dissipation, enstrophy, and the Taylor micro scale. Those quantities are all decaying with the time evolution. In order to statistically investigate how the viscoelasticity interacts with turbulence structures and influences the turbulent kinetic energy cascading procedure, a dataset of instantaneous turbulent velocity field is necessary. To this end, the FHIT is preferable to the DHIT. The stationary isotropic turbulence is often studied numerically by adding a forcing term to the Navier–Stokes equation. In several attempts of DNS of the FHIT with the presence of polymers, it was obtained that the turbulent energy cascade is deeply altered, i.e., a substantial part of the energy income does not follow the classical Kolmogorov cascade towards the viscous dissipation but is moved to the microstructures to feed an additional cascade.[26−29]

This paper presents a continuous study of the HIT influenced by the viscoelasticity. We have carried out the DNS of the FHIT at moderate Reynolds numbers with/without polymer additives. The finite elastic non-linear extensibility-Peterlin (FENE-P) model is used as the constitutive equation for the viscoelastic polymer solution. The motivation of this study is to have further insights into the DR mechanism through not only analyzing the turbulent kinetic energy spectra, the Eulerian velocity structure functions, and the small-scale turbulent vortex intermittency, but also, for the first time, analyzing the scaling law and the topological dynamics of the turbulence influenced by the viscoelasticity. Furthermore, we also aim at providing detailed information of the drag-reduced turbulence, which is valuable in developing mathematical models of drag-reducing turbulent fluid motions. This is helpful for deriving sub-grid scale models for the large eddy simulation of the drag-reducing turbulent flow by viscoelastic additives in future. In Section 2, the governing equations for the simulated FHIT of the dilute polymer solution and the numerical methods used in the DNS are described. The DNS results are presented and discussed in Section 3. Finally, we conclude our study in Section 4.

2. Governing equations and methods

The governing equations for the FHIT of a dilute polymer solution flow are

$$\frac{\partial \boldsymbol{u}}{\partial t} + \boldsymbol{u} \cdot \boldsymbol{\nabla} \boldsymbol{u} = -\frac{1}{\rho} \boldsymbol{\nabla} p + \frac{\upsilon^{[\mathrm{s}]}}{\rho} \boldsymbol{\nabla}^2 \boldsymbol{u}$$

$$+\frac{1}{\rho}\boldsymbol{\nabla}\cdot\boldsymbol{T}^{[\mathrm{p}]}+\boldsymbol{F}, \tag{1}$$

$$\frac{\partial \boldsymbol{C}}{\partial t}+\boldsymbol{u}\cdot\boldsymbol{\nabla}\boldsymbol{C}=\boldsymbol{C}\cdot\boldsymbol{\nabla}\boldsymbol{u}+\boldsymbol{\nabla}\boldsymbol{u}^{\mathrm{T}}\cdot\boldsymbol{C} -\frac{f(r)\boldsymbol{C}-\boldsymbol{I}}{\tau_{\mathrm{p}}}, \tag{2}$$

where $\boldsymbol{u}(\boldsymbol{x},t)$ is the velocity vector; $p(\boldsymbol{x},t)$ is the local pressure; $\boldsymbol{C}$ is the conformation tensor; $\boldsymbol{T}^{[\mathrm{p}]}$ is the elastic stress tensor and $\boldsymbol{T}^{[\mathrm{p}]}=\frac{\upsilon^{[\mathrm{p}]}}{\tau_{\mathrm{p}}}(f(r)\boldsymbol{C}-\boldsymbol{I})$; $\boldsymbol{I}$ is the unit tensor; ρ is the fluid density; $\upsilon^{[\mathrm{s}]}$ is the solvent kinematic viscosity; $\upsilon^{[\mathrm{p}]}$ is the polymer kinematic viscosity; τ_{p} is the polymer relaxation time; and $\boldsymbol{F}$ is the external forcing. In the FENE-P model, $f(r)=\frac{\Re^2-3}{\Re^2-r^2}$ ensures the finite extensibility, where $r^2=\mathrm{trace}(\boldsymbol{C})$ and $\Re$ are the extension length and the maximum possible extension of the polymers, respectively.

We consider the forced homogeneous isotropic turbulence, so we use 96^3 collocation points in a cubic domain (side $\ell=2\pi$ cm). We use periodic boundary conditions and solve Eq. (1) by using a standard pseudo-spectral method.[30,31] A second order Adams–Bashforth scheme is adopted for the time evolution with all the nonlinear terms fully de-aliased by the 3/2 rule.[31] For Eq. (2) in space, we use a second order central difference scheme and a second order Adams–Bashforth scheme for time marching. To guarantee the symmetrically positive and definite property of the conformation tensor $\boldsymbol{C}$ at all times and points, the Kurganov–Tadmor scheme (second-order accurate) is used in our simulations.[32]

A statistically stationary state is obtained by adding an external forcing term to Eq. (1), which acts on the largest scales by keeping their energy constant. There are many methods to add this forcing term. In this paper, we want to ensure that the energies added into the FHIT for both cases with and without polymer additives are equivalent. To do so, we choose the following procedures for the forcing term, as proposed in Ref. [33]. The stationary isotropic turbulence is maintained by using a force that keeps the total energy in each of the first two wavenumber shells ($1\le k<2$ and $2\le k<3$) constant in time; the energy spectrum is computed as $E(k)=\frac{1}{2}\sum_{S(k)}|\boldsymbol{u}(k')|^2$, where the summation $\sum_{S(k)}$ is over one wavenumber shell $k\le|k'|<k+1$, and $S(k)$ denotes the modes in the shell. We take $E_1=0.305684$ and $E_2=0.130452$.[33] At each time step, we first integrate the equations for the Fourier modes without forcing; the resulting complex Fourier modes are denoted as $u_i'(\boldsymbol{k})(t+\delta t)$. We then multiply these Fourier modes with the wavenumber between $1\le k<2$ by a constant[33]

$$u_i(\boldsymbol{k})(t+\delta t)=u_i'(\boldsymbol{k})(t+\delta t)\sqrt{E_1/E(1)(t)}, \tag{3}$$

where $E(1)(t)$ is the total energy of the modes between $1\le k<2$ calculated from $u_i'(\boldsymbol{k})(t+\delta t)$, and $u_i(\boldsymbol{k})(t+\delta t)$ is the updated Fourier amplitude. The modes in $2\le k<3$ are treated similarly.The i Initial turbulent kinetic energy spectrum $E_0(k)=0.01k^4\exp(-0.14k^2)$ is adopted.[34] The divergence-free initial velocity field $\hat{\boldsymbol{u}}_0(\boldsymbol{k})$ is generated in the Fourier space according to the Rogallo's procedure.[35] The variable with hat $\wedge$ represents that it is in the Fourier space. For the initial conformation field, $C_{ij}^0(x,y,z)=\delta_{ij}$, and the polymers are assumed to be non-stretched.[23] In the Fourier space, the turbulent kinetic energy spectrum is $E(k,t)=\frac{1}{2}\sum_{k\le k'<k+1}|\boldsymbol{u}_{k'}(t)|^2$, and the total turbulent kinetic energy is $\xi(t)=\sum_k E(k,t)$. In the physical space, $\xi(t)=\int_{\ell^3}\frac{1}{2}u_i^2(\boldsymbol{x},t)\mathrm{d}V$. The viscous dissipation in the Fourier space is $\varepsilon_\upsilon(t)=\upsilon^{[\mathrm{s}]}\sum_k k^2E(k,t)$, and in the physical space is $\varepsilon_\upsilon(t)=\int_{\ell^3}\upsilon^{[\mathrm{s}]}(\frac{\partial u_i}{\partial x_j})^2\mathrm{d}V$. For the turbulent drag-reducing flow, it is found that there exists an additional energy dissipation $\varepsilon_\tau(t)$ due to the relaxation of polymers to the equilibrium configuration.[36] The additional energy dissipation in the physical space is $\varepsilon_\tau(t)=\int_{\ell^3}f(r)T_{ii}^{[\mathrm{p}]}/(2\tau_{\mathrm{p}})\mathrm{d}V$. So, in the turbulent drag-reducing flow, the total energy dissipation is $\varepsilon_I(t)=\varepsilon_\upsilon(t)+\varepsilon_\tau(t)$.[36] The turbulent drag-reducing flow is controlled by two dimensionless parameters, the Taylor micro-scale Reynolds number $Re_\lambda=u_{\mathrm{rms}}\lambda/\upsilon^{[\mathrm{s}]}$ (where u_{rms} is the root-mean-square of the fluctuation velocity; $\lambda=u_{\mathrm{rms}}/\langle(\partial_x u_x)^2\rangle^{1/2}$ is the Taylor micro-scale) and the Weissenberg number defined as $Wi=\tau_{\mathrm{p}}/\tau_K$ (where $\tau_K=(\upsilon^{[\mathrm{s}]}/\varepsilon_\upsilon)^{1/2}$ is the Kolmogorov time scale).[36] As a reference run, we have obtained $Re_\lambda\approx 46$ for the Newtonian fluid case. The parameters for all simulations are shown in Table 1.

Table 1. The simulation parameters, where $\rho=1$ g/cm^3, $\upsilon^{[\mathrm{s}]}=0.01$ cm^2/s, $\delta t=0.001$ s, and $\Re=100$ for all simulations. The $\beta=\upsilon^{[\mathrm{s}]}/(\upsilon^{[\mathrm{s}]}+\upsilon^{[\mathrm{p}]})$ is a dimensionless measure of the polymer solution concentration, and a smaller β corresponds to a denser polymer solution. The Newtonian fluid case is also studied (run 96-E) for comparison.

Runs	τ_{p}/s	β	$(1-\beta)\Re^2/10^3$	Wi
96-A	0.1	0.9, 0.8, 0.7, 0.6	6–9	0.3
96-B	0.2	0.8, 0.6	8, 6	0.59
96-C	0.3	0.8, 0.6	8, 6	0.89
96-D	0.4	0.8, 0.6	8, 6	1.12

3. Results and discussion

It is generally accepted that forcing the Navier–Stokes equation at a low wavenumber does not influence the small scale statistics of the flow provided that there is a wide separation between the largest and the smallest scales. An important indication of the response of small scales to the forcing and of the adequate resolution of small scales is the velocity derivative skewness ($S_{\partial u} = -\langle(\frac{\partial u}{\partial x})^3\rangle/\langle(\frac{\partial u}{\partial x})^2\rangle^{\frac{3}{2}}$) that settles to a value in the neighbourhood of -0.5. This is the case for these numerical simulations, as shown in Fig. 6(a) later, indicating that the small-scale structure of the flow is uninfluenced by the forcing scheme.

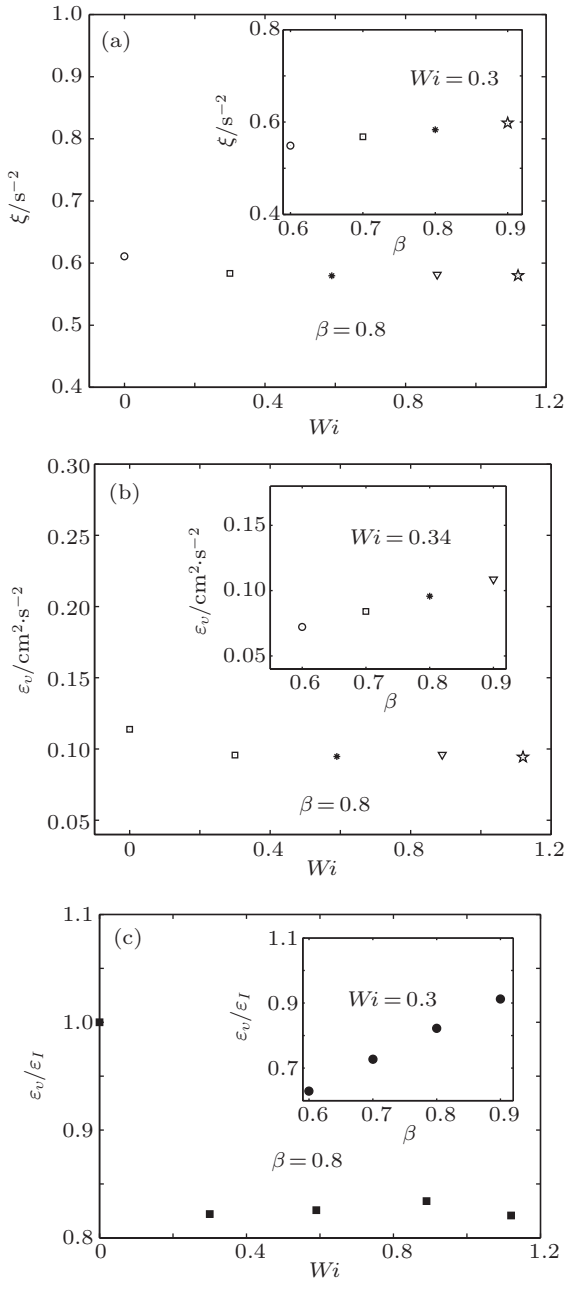


Fig. 1. (a) Turbulent kinetic energy ξ as a function of Wi and β (inset); (b) viscous dissipation ε_v as a function of Wi and β (inset); (c) viscous dissipation ε_v normalized to the total energy dissipation ε_I as a function of Wi and β (inset).

All the flow parameters reach a statistical equilibrium state after $t = 20$ s, which is about four to six times of the large-eddy turnover time ($t^{\mathrm{av}}_{\mathrm{eddy}} \approx 3$–5 s) for different simulation conditions. The statistical averages are then taken during the time period from $t = 20$ s to $t = 110$ s for all cases in our simulations. The total sampling space during this time period has 9×10^4 data points. The statistically steady values of the important turbulent parameters, such as the turbulent kinetic energy and the viscous dissipation, are shown in Figs. 1(a) and 1(b); and the viscous dissipation ε_v normalized to the total energy dissipation ε_I is shown in Fig. 1(c). It can be seen that both the turbulent kinetic energy and the viscous dissipation are decreased due to the existence of polymers. This tendency is more remarkable with the decrease of β, but is not obvious with the increase of Wi. It is possibly due to the low Wi in our simulations. The percentage remains about 82% with the increase of Wi; and it decreases with the decrease of β.

In the following sections, we shall elaborate the characteristics of the FHIT influenced by the drag-reducing polymer additives through the analyses of structural, statistical characteristics of turbulence, the turbulence scaling law, and topological dynamics, *etc.*

3.1. Statistical characteristics of FHIT influenced by polymers

The statistical characteristics of several typical turbulence quantities influenced by the drag-reducing polymers in the FHIT are investigated and elucidated as follows. Based on the analyses of the statistics in the FHIT with polymer additives, a new definition of the drag-reduction rate is then proposed for the drag-reducing FHIT.

To study the dynamics of turbulence, we have investigated the velocity gradient tensor, which governs the mechanism of vortex stretching, and in turn contributes to the energy cascade process in turbulent flows. Therefore, the evolution of the velocity gradient field is of primary importance in understanding the kinematics and the dynamics of turbulence. The velocity gradient field includes two parts, vorticity and strain. Tennekes and Lumley[37] argued that the vortex stretching is the physical mechanism leading to the hypothesized energy cascade from large to small

scales. But Tsinober[38] noted that the mechanism of the energy cascade in the physical space is not due to the vortex stretching but due to the vortex compression. He also emphasized the importance of strain as the vorticity in the context of creation and maintenance of the turbulence. Anyway, these two quantities should be considered in parallel, as they weakly correlate in the isotropic turbulence but are tied by a strongly nonlocal relation. Here we investigate the enstrophy instead of the vorticity.

To show the polymer effects, we study the polymer contribution to the enstrophy in the FHIT. Firstly, it is found that the enstrophy in the polymer solution case becomes weaker than that in the Newtonian fluid case. This tendency is the same as that in the DHIT with polymers.[24] The probability density function (PDF) of enstrophy is shown in Fig. 2. It can be clearly seen that the existence of polymers remarkably decreases the PDF of the stronger enstrophy but increases that of the weaker enstrophy, implying that the addition of polymers reduces the regions of large enstrophy and increases the regions of small enstrophy.

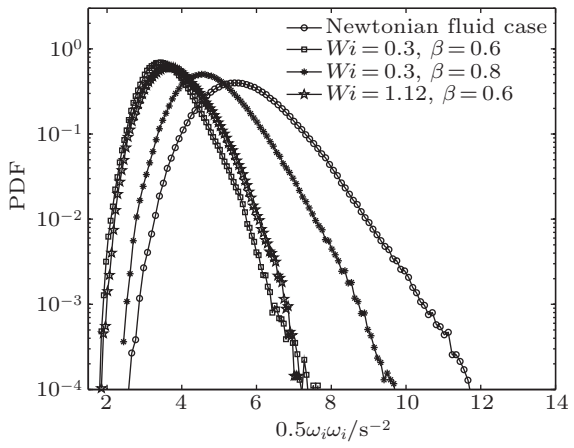


Fig. 2. PDFs of enstrophy for the Newtonian fluid and the polymer solution cases.

We have also studied the polymer effects on the strain field in the FHIT. It is found that the strain in the polymer solution case is remarkably weaker than that in the Newtonian fluid case. The existence of polymer additives also remarkably decreases the PDF of the stronger strain but increases that of the weaker strain (as shown in Fig. 3), which implies that the addition of polymers reduces the regions of large strain and increases the regions of small strain.

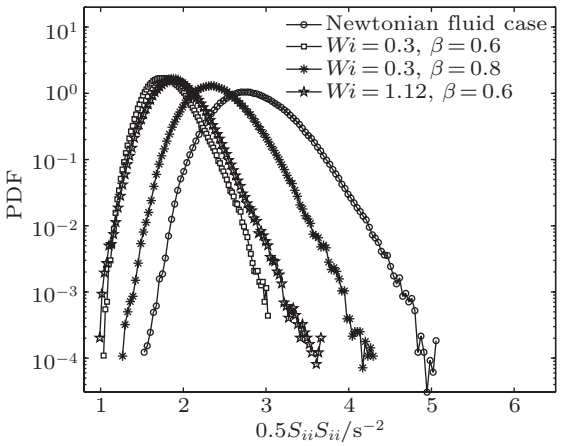


Fig. 3. PDFs of strain for the Newtonian fluid and the polymer solution cases.

To investigate the multiscale interactions between flow structures and polymer micro-structures, we pay attention to the turbulent kinetic energy spectrum $E(k)$ and the energy transfer spectrum $\Im(k)$ influenced by the polymers in the Fourier space, as shown in Fig. 4. Here $\Im(k) = \hat{\Gamma}_{ij}(\hat{T}_{ij}^{[\mathrm{p}]}) + (\hat{\Gamma}_{ij})^{*}\hat{T}_{ij}^{[\mathrm{p}]}$, $\Gamma_{ij} = \frac{\partial u_i}{\partial x_j}$, and * indicates the complex conjugate. The turbulent kinetic energy spectra attain stationarity and the distribution of energy is smooth and continuous in both the dissipation and the forced wavenumber ranges (Figs. 4(a) and 4(b)), suggesting that the forcing scheme is behaving satisfactorily in our simulations. However, the turbulent kinetic energy spectrum for the polymer solution case $E^{[\mathrm{p}]}(k)$ is apparently different from that for the Newtonian fluid case $E^{[\mathrm{N}]}(k)$: $E^{[\mathrm{p}]}(k) < E^{[\mathrm{N}]}(k)$ at large and intermediate scales and $E^{[\mathrm{p}]}(k) \gg E^{[\mathrm{N}]}(k)$ at small scales, as shown in Fig. 4(c). Besides, $E^{[\mathrm{p}]}(k)$ is nearly a constant at some scale ranges (we name such ranges as the polymer dominant scale range hereinafter). These interesting results have also been found in the other DNS results for the HIT[23,24,29] and in the experimental results for the grid turbulence.[17] In order to interpret this intriguing phenomenon, the energy transfer spectrum $\Im(k)$ by the polymers is also shown in Fig. 4(c). It is found that at large and intermediate scales, $\Im(k) > 0$, indicating that the polymers absorb the turbulent kinetic energy from the flow structures to store it as elastic energy and dissipate it by the elasticity. However, at the special polymer dominant scale range ($E^{[\mathrm{p}]}(k)$ keeps nearly a constant), $\Im(k) < 0$, adequately suggesting that the turbulent kinetic energy is transferred from the polymer micro-structures to the small-scale flow structures, and so resulting in $E^{[\mathrm{p}]}(k) \gg E^{[\mathrm{N}]}(k)$ at these scales. The addition of polymers to the FHIT provides a new route through

which the turbulent kinetic energy can flow out of the turbulence.

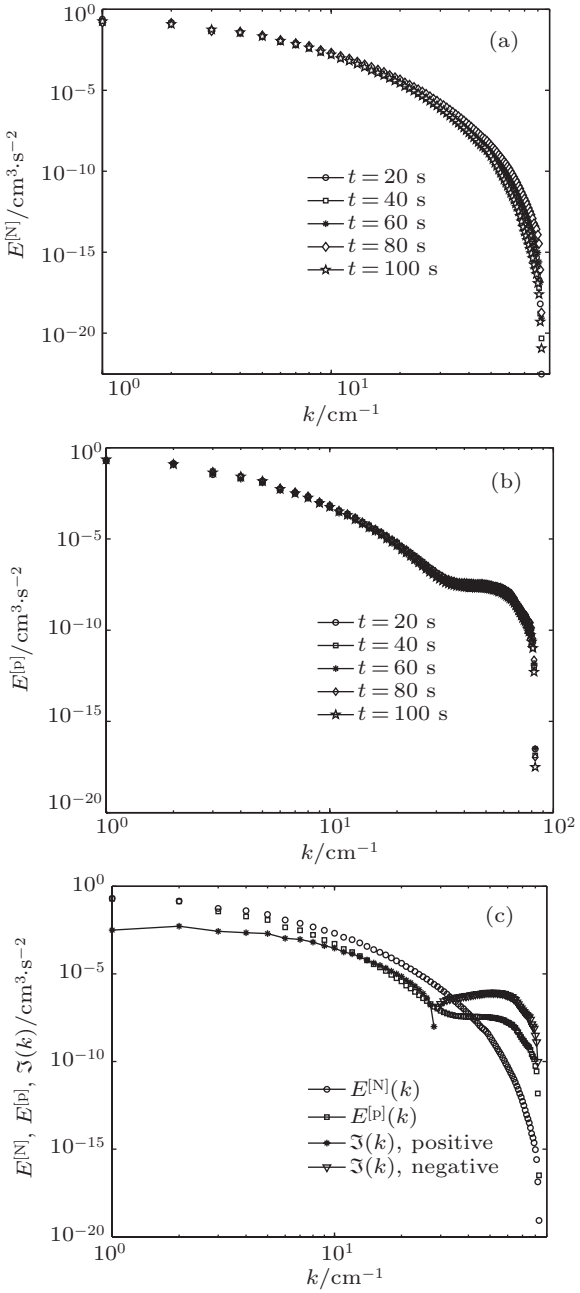


Fig. 4. Influence of turbulent kinetic energy spectrum $E(k)$ in the FHIT by polymer additives. (a) Newtonian fluid case; (b) polymer solution case, $Wi = 0.3$, $\beta = 0.6$; (c) $E(k)$ for Newtonian fluid case and $E(k)$ and $\Im(k)$ for polymer solution case, $Wi = 0.3$, $\beta = 0.6$.

Note that for the simulated viscoelastic fluid cases, the densest polymer solution corresponding to $\beta = 0.6$ has the largest viscosity. According to the definition of β, the largest viscosity of the solution is 5/3 times the viscosity of the solvent (the simulated Newtonian fluid herein) $v^{[s]}$. In order to clarify that the abovementioned phenomenon occurred in the FHIT in the polymer solution is not due to the increase of viscosity but the introduction of viscoelasticity, a numerical simulation of the FHIT in the Newtonian fluid with a viscosity of $5v^{[s]}/3$ is also performed. Figure 5 shows the turbulent kinetic energy spectrum $E(k)$ of this case as compared with the Newtonian fluid case with the viscosity of $v^{[s]}$. As expected, although $E(k)$ is depressed at larger k due to the increase of viscosity, the unique polymer dominant scale range in Fig. 4(b) cannot be realized in the Newtonian fluid cases.

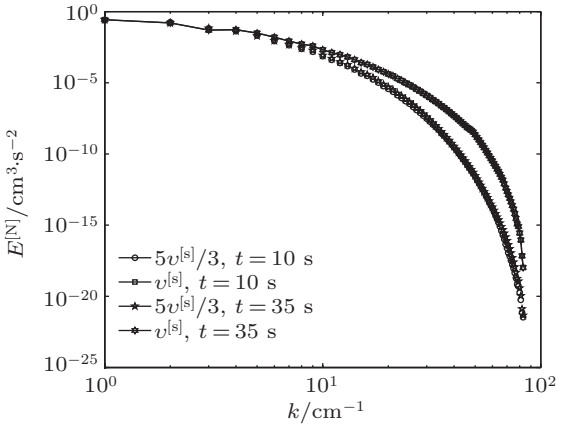


Fig. 5. Turbulent kinetic energy spectra $E(k)$ in the FHIT of Newtonian fluids with different viscosities.

To measure the modification of the turbulent energy cascade by the polymers, we use the second-order longitudinal Eulerian velocity structure function, which measures the difference in velocity over a separation $\boldsymbol{r}$, as a probe of the scale-by-scale properties of the cascade. Eulerian velocity structure functions have traditionally been used as scale-local probes of the energy cascade in the Newtonian fluid turbulence. They are defined as moments of spatial velocity differences over a separation $\boldsymbol{r}$, $\delta\boldsymbol{u}(\boldsymbol{x}) = \boldsymbol{u}(\boldsymbol{x}+\boldsymbol{r}) - \boldsymbol{u}(\boldsymbol{r})$. These velocity differences may be thought of as coarse-grained scale-local gradients. In the isotropic turbulence, the second-order structure function tensor can be parameterized by two scalar functions: a longitudinal structure function $D_{\mathrm{LL}}(r) = \langle \delta\boldsymbol{u}\delta\boldsymbol{u}\rangle$, where the velocities are taken parallel to $\boldsymbol{r}$, and a transverse structure function $D_{\mathrm{NN}}(r)$ measuring the difference in the velocity component orthogonal to $\boldsymbol{r}$. Here, we show only the results of $D_{\mathrm{LL}}(r)$. The results for $D_{\mathrm{NN}}(r)$ are similar.

Figure 6 shows that the addition of polymers has made a change to the longitudinal structure function $D_{\mathrm{LL}}(r)$, i.e., $D_{\mathrm{LL}}(r)$ is decreased at all scales investigated. This indicates the modification of the small-scale turbulence structures, and also reflects a change

of the turbulent kinetic energy transport process, especially at small-scale ranges (as shown in Fig. 4(b)). This phenomenon is consistent with the DNS results reported in Ref. [29]. Since the Taylor-scale Reynolds number is not large enough, it is hard to investigate the characteristics of larger turbulence scales. In summary, we have found that the addition of long-chain polymers strongly modifies the small-scale dynamics of turbulence even in the FHIT.

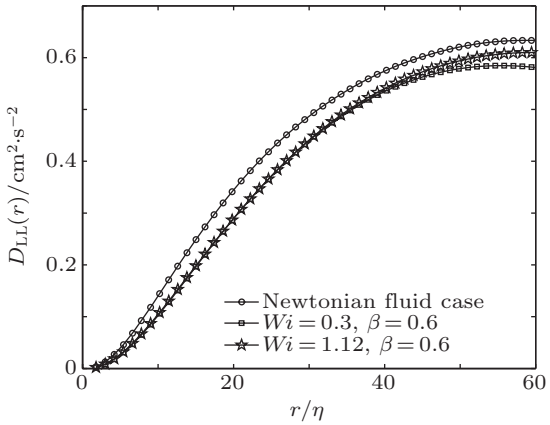


Fig. 6. The $D_{\rm LL}(r)$ versus r scaled by $\eta_{\rm w}$ (the Kolmogorov length scale determined from the water flow case).

Because the small scales of turbulence are believed to be decoupled from the large scales, what is learned about the small scales in the idealized flow FHIT, it should be applicable to turbulent flows in general. The classical approach to investigate the small-scale intermittency in turbulence is through the higher-order velocity derivative correlations, such as skewness and flatness factors. The higher-order velocity derivative correlations are defined as

$$F_{\partial u^n} = \frac{\langle(\partial u/\partial x)^n\rangle}{\langle(\partial u/\partial x)^2\rangle^{1/2n}}, \tag{4}$$

where $\langle\cdots\rangle$ represents the ensemble average. Here, when $n=3$, it represents the skewness ($F_{\partial u^3}$ or $S_{\partial u}$), when $n=4$, it represents the flatness ($F_{\partial u^4}$). As is known, for the Gaussian velocity field, $F_{\partial u^3}=0$ and $F_{\partial u^4}=3$. In our simulations, we have computed the skewness and the flatness factors of velocity derivative for the Newtonian fluid and the polymer solution cases, as shown in Fig. 7. It is shown that the skewness is in the neighbourhood of -0.5 for the Newtonian fluid and the polymer solution cases (Fig. 7(a)). The flatness factors ($F_{\partial u^4}$) suggest that the small-scale intermittency exists in the Newtonian fluid and the polymer solution cases; but the flatness factors ($F_{\partial u^4}$) in the polymer solution cases are smaller than those in the Newtonian fluid case, which indicates a suppression of the small-scale intermittency due to the addition of polymers.

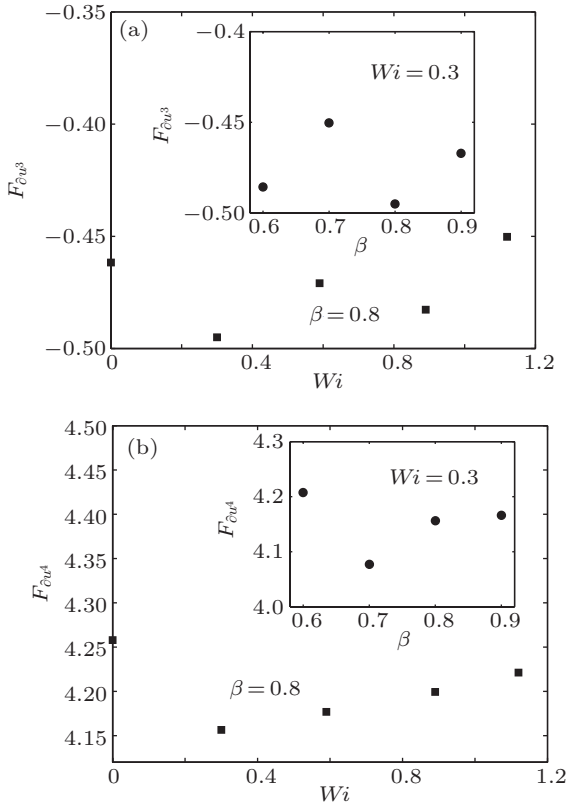


Fig. 7. (a) The skewness as a function of Wi and β (inset). (b) The flatness as a function of Wi and β (inset).

Moreover, Siggia[39] showed that in isotropic turbulence, all fourth-order velocity-derivative correlations can be expressed in terms of four rotational invariants of the velocity-deformation tensor

$$\begin{aligned} &I_1 = \langle S^4\rangle, \quad I_2 = \langle\omega^2 S^2\rangle,\\ &I_3 = \langle\omega_i S_{ij} S_{jk}\omega_k\rangle, \quad I_1 = \langle\omega^4\rangle, \end{aligned} \tag{5}$$

where

$$S_{ij} = \frac{1}{2}\left(\frac{\partial u_i}{\partial x_j} + \frac{\partial u_j}{\partial x_i}\right)$$

is the rate-of-strain tensor, $S^2 = \sum S_{ij}^2$, $S^4 = (S^2)^2$, $\omega_i = (\boldsymbol{\nabla}\times\boldsymbol{u})_i$ is the vorticity, and $\omega^2 = \sum\omega_i^2$. We normalize these correlations as follows:

$$\begin{aligned} &F_1 = \frac{15}{7}\frac{I_1}{\langle S^2\rangle^2}, \quad F_2 = 3\frac{I_2}{\langle\omega^2\rangle\langle S^2\rangle},\\ &F_3 = 3\frac{I_3}{\langle\omega^2\rangle\langle S^2\rangle}, \quad F_4 = \frac{9}{5}\frac{I_4}{\langle\omega^2\rangle^2}. \end{aligned} \tag{6}$$

In this paper, we have computed these parameters, but only shown the results of F_1 and F_4 in Fig. 8. It is shown that the flatness of enstrophy $\Omega \equiv \frac{1}{2}\omega^2$ (F_4) is larger than that of strain $\frac{1}{2}S^2$ (F_1) for the Newtonian fluid and the polymer solution cases, which

suggests that the enstrophy field is more intermittent than the strain field. It is consistent with the results of the Newtonian fluid turbulence reported in Refs. [40] and [41]. Moreover, all four high-order velocity derivative correlations in each of the simulated polymer solution cases are smaller than their Newtonian fluid counterpart.

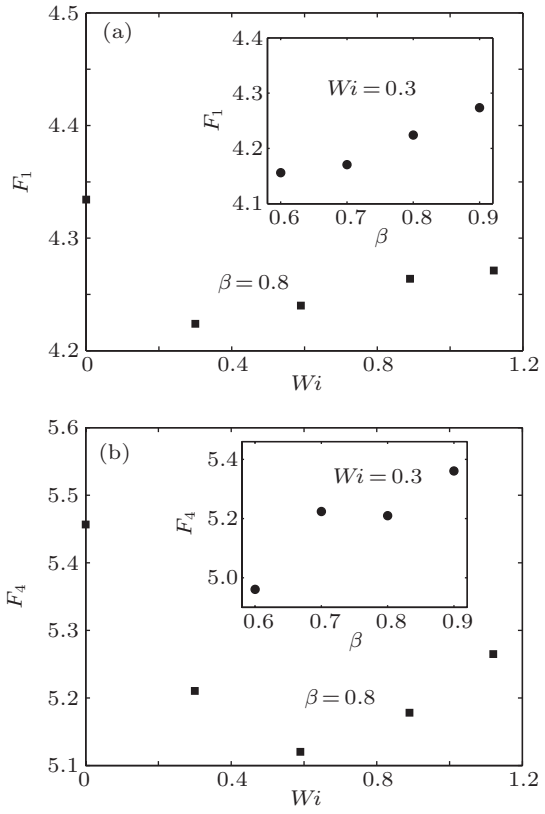


Fig. 8. The flatness of strain as a function of Wi and β (inset). (b) The flatness of enstrophy as a function of Wi and β (inset).

The DR phenomenon in wall-bounded turbulent flows has been well documented through a large number of experimental and numerical simulation studies. The typical characteristics of turbulent vortex structures and turbulence statistics appeared in drag-reducing wall-bounded turbulent flows, as described previously in Section 1, are directly related to the wall effects or the inhomogeneous nature of the wall flows. However, the HIT removes the inhomogeneous nature (no wall effect), and only involves the transfer of the turbulent kinetic energy without the change of the momentum fluxes. This straightforwardly results in some different mechanisms for the DR phenomenon in the HIT as compared with those in wall-bounded turbulent flows.

In the DHIT, the initial exerted energy is merely the initial turbulent kinetic energy. The larger decay rate of the turbulent kinetic energy represents a more remarkable inhibition of turbulence and a stronger tendency of making the flow regular. It is analogous to the drag-reducing effect in wall-bounded turbulent flows. Thus, we have proposed a definition of the DR rate for the DHIT with polymer additives based on the statistical kinetic energy decay.[24] But in the FHIT, the initial exerted energy is the sum of the additional forcing energy and the initial turbulent kinetic energy. According to the above analyses for wall-bounded and HIT flows, the addition of additives also decreases the turbulent kinetic energy so as to decrease the turbulent energy dissipation. Hence, we propose here an intuitive and natural definition for the DR rate occurred in the FHIT based on the decreased degree of the turbulent kinetic energy

$$\mathrm{DR}(\%) = \frac{\Delta\xi^{[\mathrm{p}]} - \Delta\xi^{[\mathrm{N}]}}{\Delta\xi^{[\mathrm{N}]}} \times 100\%, \tag{7}$$

where $\Delta\xi = (\xi_{\mathrm{F}} + \xi_{\mathrm{ini}}) - \xi_{\mathrm{eq}}$, ξ_{F}, ξ_{ini}, and ξ_{eq} represent the additional forcing energy ($\xi_{\mathrm{F}} = E_1 + E_2$), the initial turbulent kinetic energy ($\xi_{\mathrm{ini}} = \sum_k E_0(k,t)$), and the turbulent kinetic energy at the statistical equilibrium state for each case ($\xi_{\mathrm{eq}} = \sum_k E(k,t)$), respectively. Here, superscripts N and p represent the Newtonian fluid and the polymer solution cases, respectively.

The DR versus β is plotted in Fig. 9 for the polymer solution case at $Wi = 0.3$. It is shown that the DR rate increase with the decrease of β, i.e., with an increase of the solution concentration. But, there is no clear dependence on Wi for the DR rate in the FHIT in our simulated cases.

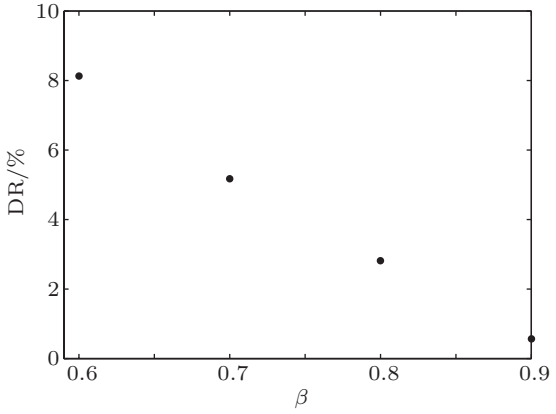


Fig. 9. The DR rate versus β in the FHIT with polymer additives, $Wi = 0.3$.

3.2. Characteristics of polymer stretching and turbulence structure in the FHIT with polymer additives

In the FHIT with polymer additives, a part of the forcing energy should be inevitably shared for maintaining the population of stretched polymer molecules (as indicated in the turbulent kinetic energy spectrum shown in Figs. 4(b) and 4(c)), which slightly reduces the energy available for turbulent fluctuation (as shown in Fig. 1(a)). The conformation field of the polymer solution containing the information of the polymer molecule stretching degree reflects how much energy the polymers absorb. We then investigated such information as follows.

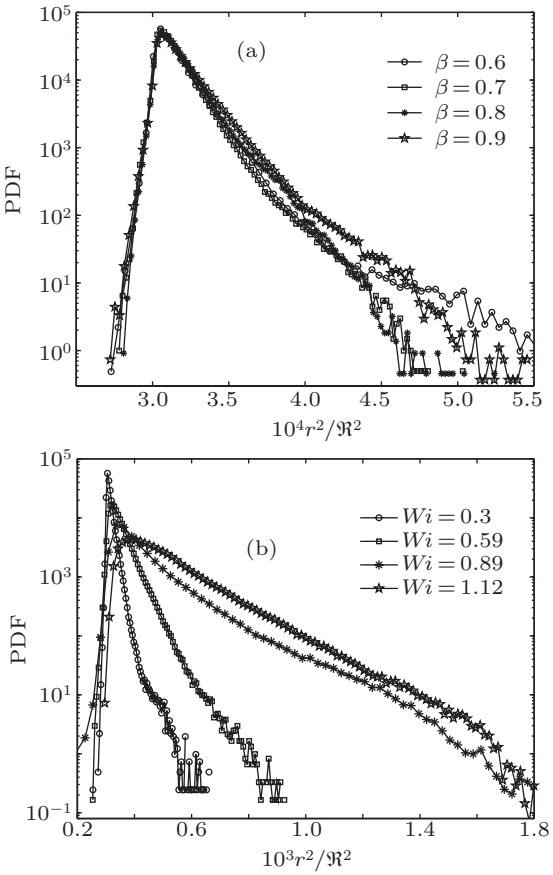


Fig. 10. The PDFs of $r^2/\Re^2$ for (a) four different β at $Wi = 0.3$ and (b) four different Wi at $\beta = 0.6$.

Figure 10 shows the PDF of the polymer stretching $r^2/\Re^2$. It can be seen that the polymer stretching changes a little with β; with the increase of Wi, the peak of the PDF curve becomes lowered and shifts towards the larger stretching. In order to evaluate the overall polymer stretching, we have obtained the ensemble average of $r^2/\Re^2$ for different β and Wi, as shown in Fig. 11. The ensemble average of $r^2/\Re^2$ increases with the increase of β. The reason is that for a larger concentration, a more remarkable DR occurs, and at the same time, the mean velocity gradient generated by the turbulent fluctuation becomes weakened, leading to a smaller polymer stretching (Fig. 11(a)). However, it is shown that the ensemble average of $r^2/\Re^2$ increases with the increase of Wi at the same concentration.

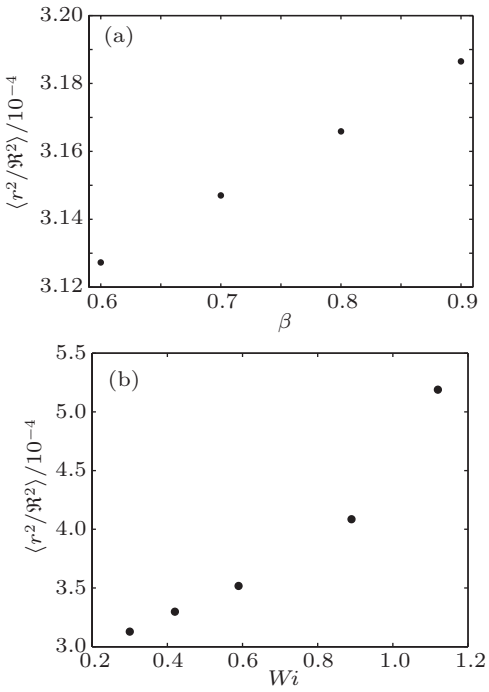


Fig. 11. The ensemble averages of $r^2/\Re^2$ for (a) four different β at $Wi = 0.3$ and (b) four different Wi at $\beta = 0.6$.

As is known, the existence of coherent structures is one of the most important characteristics in turbulence, and the coherent structures can be divided into two groups: tube-like vortex structures and sheet-like vortex structures. They undoubtedly play an important role in the overall dynamics and kinematics of turbulence. The tube-like vortex structures are mostly responsible for the generation of intermittency. The sheet-like vortex structures are those regions in which the rate-of-strain and the vorticity are highly correlated with each other and comparably equal in their magnitudes. A considerable dissipation of the turbulent kinetic energy, which is the final result of the energy cascade, takes place in the sheet-like vortex structures. The introduction of polymers can signifi-

cantly modify the dynamic behaviour and the properties of the coherent structures, which is closely related to the DR mechanism. Therefore, extracting the coherent structures from the FHIT with/without polymer additives is a fundamental and intuitive way to investigate how the polymer additives interact with the turbulence structures.

Up to now, several methods have been considered for visualizing the tube-like vortex structures based on the second invariant Q, discriminant Δ, or eigenvalues (λ_2, λ_{ci}) of the velocity gradient tensor $\boldsymbol{\nabla u}$.[42] In this paper, we use the invariant Q method to extract the tube-like vortex structures in the FHIT, as briefly described below.

Three invariants for velocity gradient tensor $\nabla \boldsymbol{u}$ are

$$P = S_{ii}, \quad Q = (P^2 - S_{ij}S_{ji} - W_{ij}W_{ji})/2,$$
$$R = (-P^3 + 3PQ - S_{ij}S_{jk}S_{ki} - 3W_{ij}W_{jk}W_{ki})/3, \quad (8)$$

where

$$W_{ij} = (\partial u_i/\partial x_j - \partial u_j/\partial x_i)/2$$

is the rate-of-rotation tensor. For the incompressible flow, we have

$$P = 0, \quad Q = (W_{ij}W_{ij} - S_{ij}S_{ij})/2,$$
$$R = (-S_{ij}S_{jk}S_{ki} - 3W_{ij}W_{jk}S_{ki})/3. \quad (9)$$

The second invariant Q reflects the relative strength of the rate-of-rotation and rate-of-strain. The positive Q isosurfaces isolate the areas where the strength of the rate-of-rotation is larger than that of the rate-of-strain, thus a tube-like zone can be defined as the region with positive Q isosurfaces. The analysis results for the vortex tube structures are shown in Fig. 12.

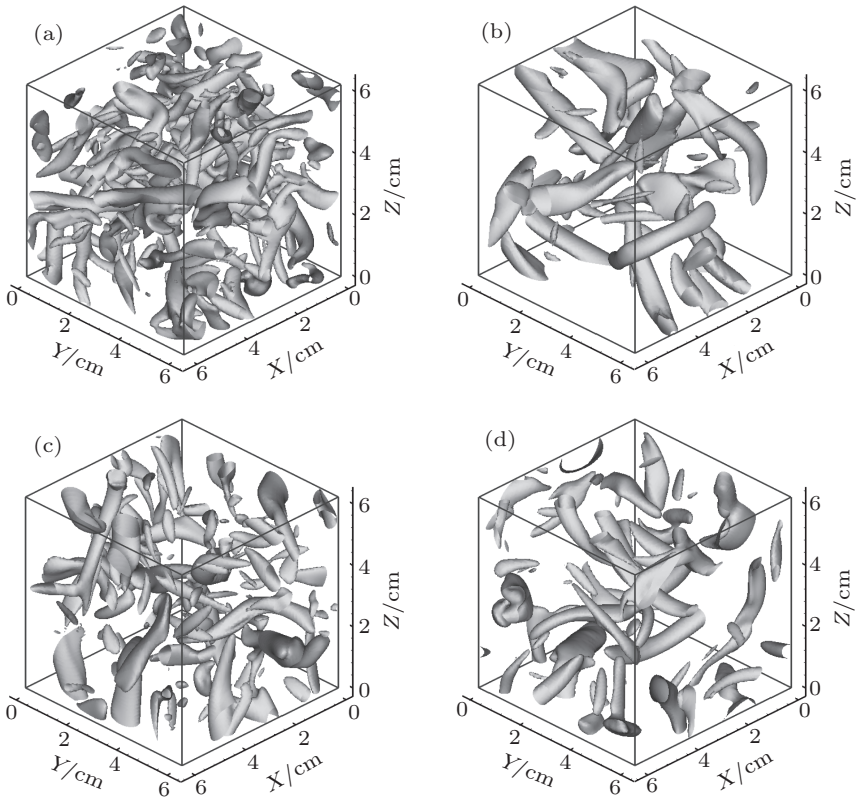


Fig. 12. (colour online) Constant Q isosurfaces ($Q = 3$) for (a) the Newtonian fluid case; (b) $Wi = 0.3$, $\beta = 0.6$; (c) $Wi = 0.3$, $\beta = 0.8$; (d) $Wi = 1.12$, $\beta = 0.6$.

However, unlike tube-like vortex structures, very few identification methods for sheet-like vortex structures have been proposed. Because the sheet-like vortex structures are more disorganized than the tube-like vortex structures, it is fairly difficult to examine them in turbulent flows. Recently, Horiuti and

Takagi[43] proposed a new definition for vortex sheets based on the eigen-decomposition of the symmetric second-order velocity gradient tensor. Since, the eigenvalues of A_{ij} are obtained from the equation

$$x^3 - (A_{ij}A_{ji})x/2 - A_{ij}A_{jk}A_{ki}/3 = 0. \tag{10}$$

Then, we use $[A_{ij}]_z$, $[A_{ij}]_+$, and $[A_{ij}]_-$ to denote the eigenvalue associated with the eigenvector that is maximally aligned with the velocity vector, the largest remaining and the smallest eigenvalues, respectively. It is observed that vortex sheets can be examined based on the criterion

$$[A_{ij}]_+ > \{[A_{ij}]_+\}_{\rm th}, \tag{11}$$

where $\{[A_{ij}]_+\}_{\rm th}$ is an arbitrary positive threshold. In this paper, we use this method to identify the vortex sheets in the FHITs of both the Newtonian fluid and the polymer solution, and the results are shown in Fig. 13.

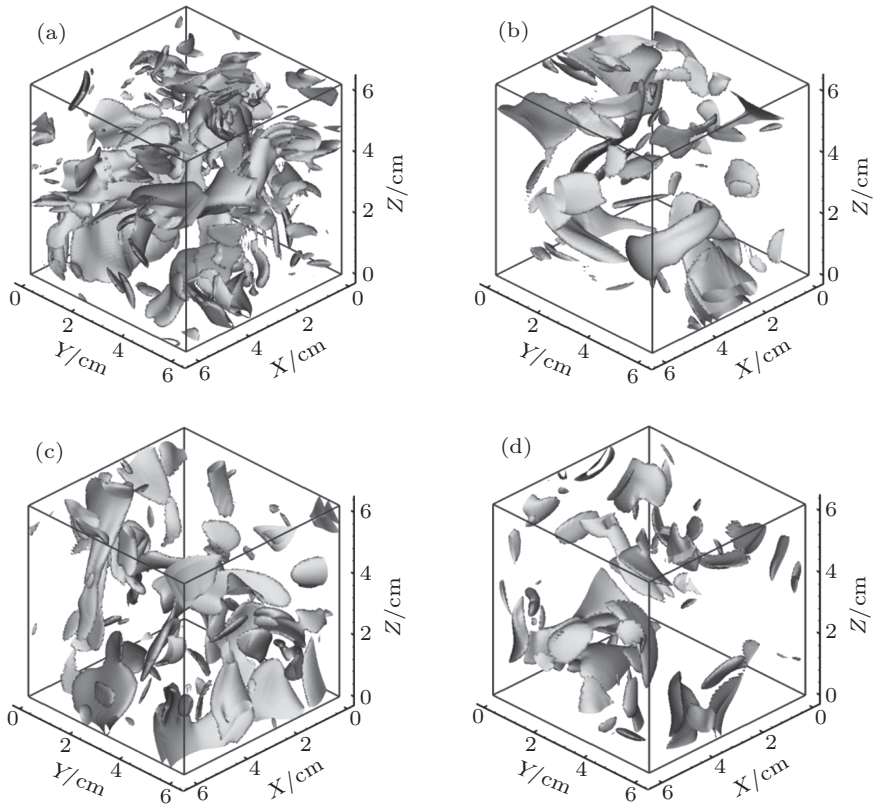


Fig. 13. Constant $[A_{ij}]_+$ isosurfaces ($[A_{ij}]_+ = 10$) for (a) the Newtonian fluid case; (b) $Wi = 0.3$, $\beta = 0.6$; (c) $Wi = 0.3$, $\beta = 0.8$; (d) $Wi = 1.12$, $\beta = 0.6$.

Figure 12 shows that as compared with the Newtonian fluid case, much less but wider tube-like vortex structures are present in the FHIT for the polymer solution cases. This appearance of vortex tube structures also reflects a decrease in enstrophy, since the enstrophy indicates the strength of the tube-like vortex structures and mainly is generated by the stretching of the tube-like vortex structures. This result is consistent with the DNS results of the HIT with polymer additives in Ref. [27]. Moreover, this phenomenon is more remarkable with decreases of β and Wi. By visualizing the sheet-like vortex structures in Fig. 13, it is clearly seen that the addition of polymers can cause a significant depression of the sheet-like vortex structures. There are only larger sheet-like vortex structures in the polymer solution cases. In the sheet-like vortex structure regions, the polymer effects are dominant. It is because the distribution of polymer elastic energy is primarily concentrated along the sheet-like vortex structure, resulting in a depression of the local

vortex structures. It is qualitative to say that tube-like and sheet-like vortex structures are both important for energy dissipation and cascade, and their depressions imply the decrease of viscous dissipation (Fig. 1(b)) and the modification of energy cascade (Fig. 4) to some extent in the FHIT.

3.3. Turbulence scaling law in FHIT influenced by polymers

The scaling of the velocity structure functions in the turbulent flow plays a very important role in the statistical physics of turbulence, and the existence of scaling is an indication of scale invariance in turbulence. The p-th order structure function is defined as the p-th order moment of velocity increments at scale r[44]

$$S_p(r) = \langle |\delta \boldsymbol{u}(r)|^p \rangle = \langle |\boldsymbol{u}(\boldsymbol{x}+r) - \boldsymbol{u}(\boldsymbol{x})|^p \rangle. \quad (12)$$

At a scale r satisfying $L > r \gg \eta$ and $\eta = (\upsilon^3/\varepsilon)^{1/4}$, the scaling law of the structure function might exist

$$S_p(r) \propto r^{\zeta(p)}. \quad (13)$$

The Kolmogorov theory (K41) gives the scaling exponent $\zeta(p) = p/3$, which has been modified with consideration of the intermittency of turbulence.

The scaling law is obvious at the inertial range only for high-Reynolds-number turbulent flows. At a low or moderate Reynolds number, the scaling law is either indiscernible or valid in a very small internal of r. Benzi *et al.*[44] first proposed the so-called extended self-similarity (ESS), establishing an extended region (beyond the traditional inertial range) of the observed scale similarity. Formally, the ESS refers to

$$S_p(r) \propto S_q(r)^{\zeta(p)/\zeta(q)}. \quad (14)$$

Since in K41, $\zeta(3) = 1$, $q = 3$ is thus usually used in the ESS, i.e.,

$$S_p(r) \propto S_3(r)^{\zeta(p)}. \quad (15)$$

Benzi *et al.*[44] showed that with the same scaling exponents of fully developed turbulence, equation (15) is valid not only for high-Reynolds-number turbulent flows, but also for moderate- or low-Reynolds-number turbulent flows, in which the scaling law according to Eq. (13) is invisible.

As is known, the drag-reducing turbulent flow by polymers is still in the turbulent flow state but with modified turbulence characteristics. We then explore the scaling laws of the structure functions in a fashion of ESS in the FHIT with polymer additives as a typical example of the simulated viscoelastic fluid cases, as depicted in Figs. 14(b) and 15(b), in order to further understand the turbulent DR phenomenon as well as shed light on the essence of turbulence. To the best of our knowledge, this is the first time the scaling properties of the velocity structure functions for a drag-reducing turbulent flow have been investigated.

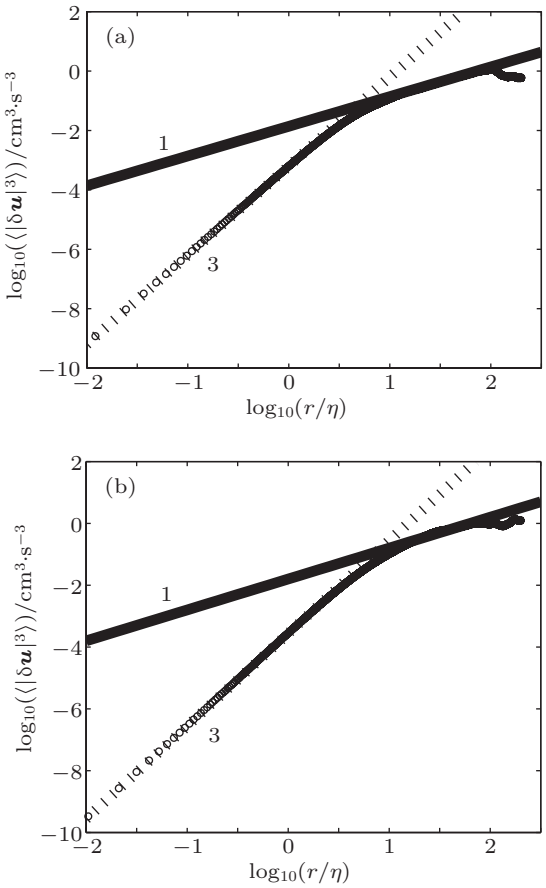


Fig. 14. Log–log plot of $S_3(r)$ versus r/η for (a) the Newtonian fluid; (b) $Wi = 0.3$, $\beta = 0.6$ as a typical example of the simulated viscoelastic fluid cases.

The simplest way to detect the existence of an inertial range in the fully developed turbulence is to check whether the third order structure function is proportional to r for large enough values of r (in any case smaller than the integral scale L). From Fig. 14, it is clearly seen that there exists a remarkable inertial range for the Newtonian fluid case, but the iner-

tial range has been shortened in the polymer solution cases. We also find that for very small scales, the velocity difference is regular, i.e., $\delta \boldsymbol{u}(r)$ is proportional to r for $r \ll \eta$ (dashed straight line shown in Fig. 14). For the other structure functions in different orders, similar phenomena can be observed for the Newtonian fluid and the polymer solution cases.

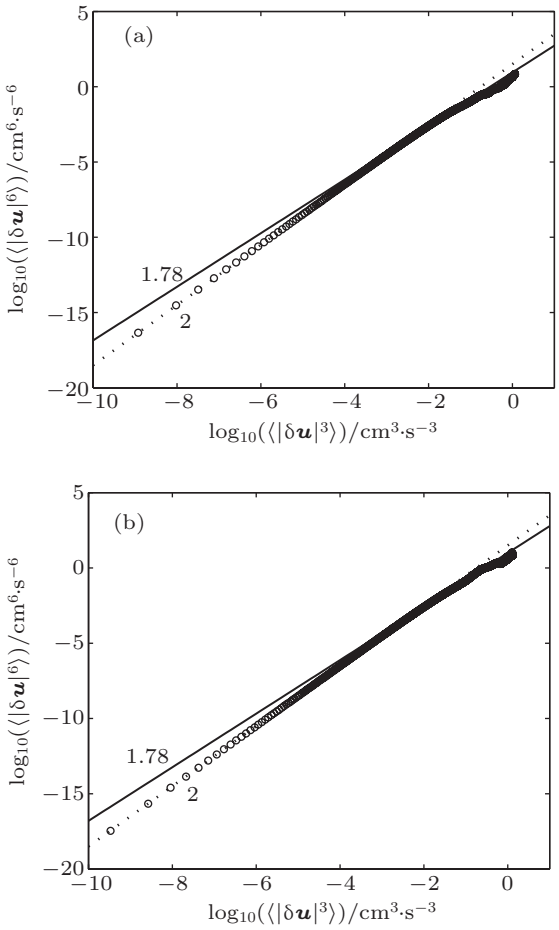


Fig. 15. Log–log plot of $S_6(r)$ versus $S_3(r)$for (a) the Newtonian fluid; (b) $Wi = 0.3$, $\beta = 0.6$ as a typical example of the simulated viscoelastic fluid cases.

In Fig. 15, we show the scaling law in a fashion of ESS, depicting the log–log plot of the six-order structure function against the third-order one. We find two different regions of scaling: a region of anomalous scaling for greater than approximately 4η (ESS as discussed in the previous section) and a region of the scaling exponent asymptotically equaling to 2 for scales smaller than η. It is striking to see that there is no distinct difference between the scaling laws for the Newtonian fluid and the drag-reducing polymer solution cases. This might be either the real situation or due to Wi of all simulated FHITs for the polymer solution cases being still too low (or the DR rate being too small) to get an obviously different scaling law for drag-reducing turbulence. This issue calls for a further and much more detailed exploration.

3.4. Topological dynamics analysis of FHIT with/without polymer additives

As mentioned above, Q in Eq. (9) represents the relative strength of enstrophy and strain (i.e., enstrophy dominated versus strain dominated regions), and R represents the relative strength of enstrophy and strain production (i.e., vortex stretching versus vortex compression). Since the invariants Q and R are scalar quantities, their values are independent of the coordinate orientations and contain information concerning the rates of vortex stretching and rotation. Thus, the so-called local flow topological dynamics methodology,[45] i.e., analysis of the Q–R invariant map, has been a useful tool for investigating small-scale vortex motions in turbulent flows.

The topological dynamics analysis for the velocity gradient tensor of the FHIT with/without polymer additives has been performed in this paper to explore the effect of viscoelasticity on the turbulence structures. Through the analysis of the physical meanings represented by Q and R, clear physical images for the topological dynamics characteristics can be obtained, such as the scatter plots of Q and R shown in Fig. 16. It can be seen that R and Q are mainly concentrated around the origin of coordinates for the Newtonian fluid and the polymer solution cases, indicating a relatively small velocity gradient in the large part of the flow field. The typical teardrop shape of the R–Q plots remains qualitatively unchanged for the Newtonian fluid case and the polymer solution cases, indicating that most of the flow fields are covered with the SF/S (stable-focus/stretching) and the UN/S/S (unstable-node/saddle/saddle) topological structures. There also exist four topological flows in the FHIT of the polymer solution. This interesting phenomenon is consistent with the DNS results reported in Ref. [29]. However, it can be seen that the tails of the teardrop shapes have been changed for the polymer solution cases compared with its Newtonian fluid counterpart: the large-R and Q regions have shrunk greatly, which indicates the inhibition of small-scale vortices. This

structure change is noteworthy because the tail corresponds to the flow situations dominated by strain as compared with enstrophy and by the production of strain as compared with the production of enstrophy. This phenomenon, again, demonstrates that the strain, the enstrophy, their production, and the sheet-like vortex structures in the FHIT have been significantly changed by the polymer additives.

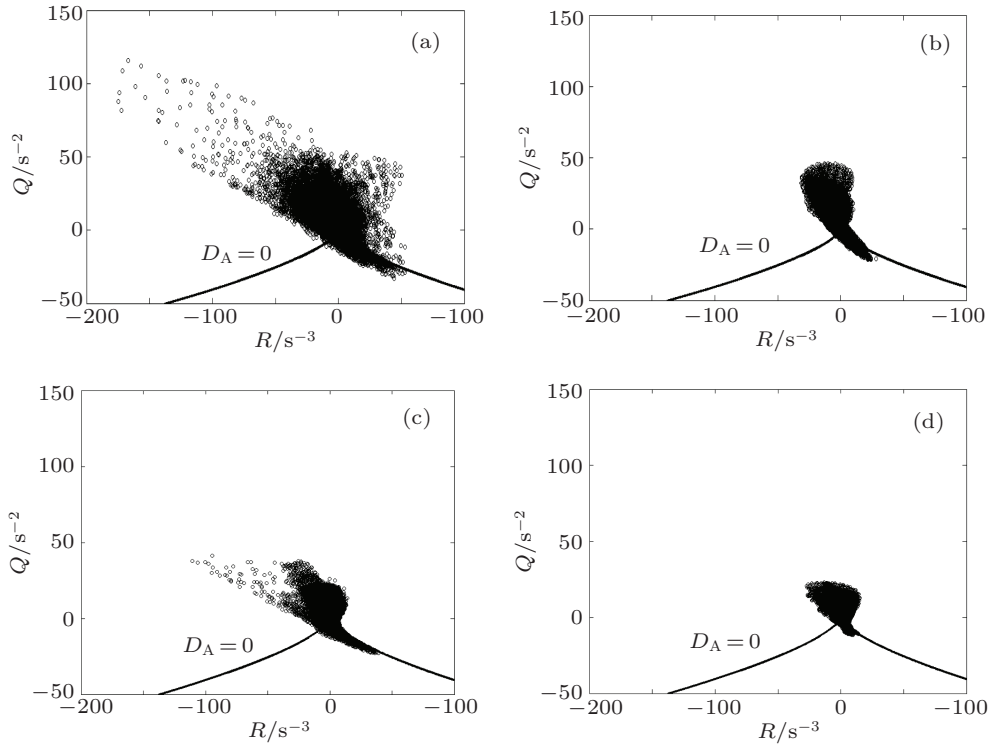


Fig. 16. Joint PDFs of the normalized second (Q) and third (R) invariants of the velocity gradient tensor. (a) the Newtonian fluid case; (b) $Wi = 0.3$, $\beta = 0.6$; (c) $Wi = 0.3$, $\beta = 0.8$; (d) $Wi = 1.12$, $\beta = 0.6$. The tent-like curve on the figure is the discriminant $D_A = 27R^2/4 + Q^3 = 0$ line.

4. Conclusions

The DNS of FHIT with and without polymer additives have been carried out based on the Navier–Stokes equation coupled with the FENE-P model. Several conclusions have been drawn from the detailed analyses of the DNS results as follows:

1) The most important turbulent parameters of the FHIT with polymer additives, such as the turbulent kinetic energy and the energy dissipation rate, have been remarkably altered by the drag-reducing polymer additives.

2) An intuitive and natural definition for the DR rate occurred in the FHIT of the polymer solution has been proposed based on the decrease degree of the turbulent kinetic energy. Such a DR rate increases with the increase of the solution concentration, while there is no clear dependence on Wi in the present simulations.

3) Turbulent kinetic energy spectra $E(k)$ and energy transfer spectrum $\Im(k)$ between the turbulent structures and the polymer micro-structures in the FHIT of polymer solution show that $E^{[N]}(k) > E^{[p]}(k)$ at large and intermediate scales and $E^{[p]}(k) \gg E^{[N]}(k)$ at small (polymer dominant) scales due to the role of $\Im(k)$. It indicates that the classical turbulent kinetic energy cascade is significantly modified due to the polymer effects.

4) The flatness factor of the velocity gradient shows that the small-scale intermittency in the FHIT is suppressed by the polymer additives. The visualization of vortex structures demonstrates that the complexities of both tube-like and sheet-like vortices in the FHIT of polymer solution have been greatly inhibited due to the polymer effects.

5) The scaling law of turbulence in a fashion of ESS in the FHIT of polymer solution shows similar features compared with that of the Newtonian fluid. This might be the case or it could be due to the Wi of all presently simulated FHIT of the polymer solution

being still too low to get an obviously different scaling law for the drag-reducing turbulence. This should remain open and calls for further investigations.

6) The enstrophy and the strain in the FHIT of the polymer solution are both remarkably weaker than those of the Newtonian fluid. The addition of polymers remarkably decreases the PDF of the stronger enstrophy/strain (reduces the regions of large enstrophy/strain) but increases the PDF of the weaker enstrophy/strain (increase the regions of small enstrophy/strain).

7) The topological dynamics analysis for the velocity gradient tensor of the FHIT shows that the typical teardrop shape of the R–Q plots remains qualitatively unchanged for the Newtonian fluid case and the polymer solution cases. Quantitatively, however, the large-R and Q regions have shrunk greatly for the polymer solution cases compared with its Newtonian fluid counterpart, indicating the inhibition of small-scale vortices.

Acknowledgements

We thank Prof. Yu of China University of Petroleum (Beijing) and Dr. Yamamoto of Kyoto University for their discussion on the DNS. The authors are very grateful to the enthusiastic help of all members of Complex Flow and Heat Transfer Laboratory of Harbin Institute of Technology.

References

[1] Toms B A 1949 *Proceedings of the First International Congress of Rheology* (Amsterdam: North Holland) p. 135
[2] Lumley J L 1973 *J. Polymer Sci. Macrom. Rev.* **7** 263
[3] Virk P S 1975 *AIChE J.* **21** 625
[4] Walker D T and Tiederman W G 1990 *J. Fluid Mech.* **218** 377
[5] Sreenivasan K R and White C M 2000 *J. Fluid Mech.* **409** 149
[6] Liberatore M W, Baik S, McHugh A J and Hanratty T J 2004 *J. Non-Newtonian Fluid Mech.* **123** 175
[7] Li F C, Kawaguchi Y, Segawa T and Hishida K 2005 *Phys. Fluids* **17** 075104
[8] Li F C, Kawaguchi Y, Hishida K and Oshima M 2006 *Exp. Fluids* **40** 218
[9] Li F C, Yu B, Wei J J, Kawaguchi Y and Hishida K 2008 *Int. J. Heat Mass Transfer* **51** 835
[10] Groisman A and Steinberg V 2000 *Nature* **405** 53
[11] Groisman A and Steinberg V 2004 *New J. Phys.* **6** 1
[12] Li F C, Kinoshita H, Li X B, Oishi M, Fujii T and Oshima M 2010 *Exp. Thermal Fluid Sci.* **34** 20
[13] Hetsroni G, Zakin J L and Mosyak A 1997 *Phys. Fluids* **9** 2397
[14] Warholic M D, Schmidt G M and Hanratty T J 1999 *J. Fluid Mech.* **388** 1
[15] Ptasinski P K, Boersma B J, Nieuwstadt F T M, Hulsen M A, Van den Brue B H A A and Hunt J C R 2003 *J. Fluid Mech.* **490** 251
[16] Li F C, Kawaguchi Y and Hishida K 2004 *Phys. Fluids* **16** 3281
[17] Fabula A G 1966 *An Experimental Study of Grid Turbulence in Dilute High-polymer Solutions* (Ph.D. Thesis) (State College: The Pennsylvania State University)
[18] McComb W D, Allan J and Greated C A 1977 *Phys. Fluids* **20** 873
[19] Friehe C A and Schwarz W H 1970 *J. Fluid Mech.* **44** 173
[20] van Doorn E, White C M and Sreenivasan K R 1999 *Phys. Fluids* **8** 2387
[21] Barnard B J and Sellin R H J 1969 *Nature* **222** 1160
[22] Kalelkar C, Govindarajan R and Pandit R 2005 *Phys. Rev.* E **72** 017301
[23] Perlekar P, Mitra D and Pandit R 2006 *Phys. Rev. Lett.* **97** 264501
[24] Cai W H, Li F C and Zhang H N 2010 *J. Fluid Mech.* **665** 334
[25] Cai W H, Li F C and Zhang H N 2011 *Chin. Phys.* B **20** 1
[26] Vaithianathan T and Collins L R 2003 *J. Comput. Phys.* **187** 1
[27] De Angelis E, Casciola C M, Benzi R and Piva R 2005 *J. Fluid Mech.* **531** 1
[28] Jin S 2007 *Numerical Simulations of a Dilute Polymer Solution in Isotropic Turbulence* (Ph.D. Thesis) (Ithaca: Cornell University)
[29] Perlerkar P, Mitra D and Pandit R 2010 *Phys. Rev.* E **82** 066313
[30] De Angelis E, Casciola C M, Benzi R and Piva R 2002b *Chaodyn-nlin.* 0208016 1
[31] Canuto C, Hussaini M Y, Quarteroni A and Zang T A 1988 *Spectral Methods in Fluid Dynamics* (New York: Spring-Verlag) p. 505
[32] Kurganov A and Tadmor E 2000 *J. Comp. Phys.* **160** 241
[33] Chen S Y, Doolen G D and Kraichnan R H 1993 *Phys. Fluids* **5** 458
[34] Sullivan N P, Mahalingam S and Kerr R M 1994 *Phys. Fluids* **6** 1612
[35] Rogallo R S 1981 *Technical Report No.81315*, NASA
[36] Berti S, Bistagnino A, Boffetta G, Celani A and Musacchio S 2006 *Europhys. Lett.* **76** 63
[37] Tennekes H and Lumley J L 1972 *A First Course in Turbulence* (Cambridge: MIT Press) p. 103
[38] Hunt J C R and Vassilicos 2000 *Turbulence Structure and Vortex Dynamics* (New York: Cambridge University Press) p. 164
[39] Siggia E D 1981 *Phys. Fluids* **24** 1934
[40] Siggia E D 1981 *J. Fluid Mech.* **107** 375
[41] Kerr R M 1985 *J. Fluid Mech.* **153** 31
[42] Horiuti K and Takagi Y 2001 *Phys. Fluids* **13** 3756
[43] Horiuti K and Takagi Y 2005 *Phys. Fluids* **17** 121703
[44] Benzi R, Ciliberto S, Tripiccione R, Baudet C, Massaioli F and Succi S 1993 *Phys. Rev.* E **48** R29
[45] Perry A E and Chong M S 1987 *Annu. Rev. Fluid Mech.* **19** 125